Multiple Liquefaction of Granular Soils: A New Stacked Ring Torsional Shear Apparatus and Discrete Element Modeling

Duruo Huang[1*], Zhengxin Yuan[2], Siyuan Yang[1], Pedram Fardad Amini[2], Gang Wang[2], Feng Jin[1]

[1] Tsinghua University, Beijing 100084, China
[2] Hong Kong University of Science and Technology, Clear Water Bay, Kowloon, Hong Kong

[*] Corresponding author: huangduruo@tsinghua.edu.cn

Abstract: In this study, we develop an innovative stacked ring torsional shear apparatus for multiple liquefaction tests of fully saturated sands. Stacked rings are built upon an existing hollow cylinder torsional shear apparatus to impose lateral constraint to the soil sample, such that multiple liquefaction can be tested in a fully saturated state. In this project, we used pressure compensation technique to reduce vertical friction between the sample and the ring direct contact force between the membrane and the rings such that the vertical stress will be much more uniformly distributed along the sample height. The new stacked ring device facilitates investigation of fabric evolution and its effect on reliquefaction resistance of sands.

To further study the fundamental mechanism of the multiple liquefaction phenomenon, 3D clumped discrete model is used to construct realistic particle packings, and simulate fabric evolution during liquefaction-reconsolidation-reliquefaction process. The study reveals that strain history significantly influences the number of inter-particle contact and fabric anisotropy after reconsolidation, hence the subsequent liquefaction resistance greatly varies. The increase in relative density due to reconsolidation has only secondary effects. The state-of-the-art DEM simulation provides micromechanical insights into the fundamental mechanism of the multiple liquefaction phenomenon.

Keywords: Multiple Liquefaction, Stacked Rings, Laboratory Tests, Discrete Element Model.

1 Introduction

Liquefaction is a phenomenon in which saturated soils suffer from substantial loss of strength and stiffness induced due to the shear strains during seismic shaking. In the past several decades, liquefaction has always been a significant subject in geotechnical engineering because of the tremendous destructive capacity to infrastructures causing serious economic losses and deaths [1]. Reliquefaction or multiple liquefaction refers to the repeated occurrence (twice or more) of soil liquefaction at the same location

during a sequence of earthquake events. The resistance of sands to a subsequent liquefaction event may tend to decrease, even if the sample possesses a higher relative density after being fully consolidated due to the pore pressure dissipation. Multiple liquefaction events have been recorded in all over the world, for example, 1983 Nihonkai-Chubu earthquake [2], 2011 Tohoku earthquake in Japan [3], and from September 2010 to December 2011 in the city of Christchurch, New Zealand [4]. In recent years, studying multiple liquefaction resistance of soils has received great attention within the geotechnical community.

Triaxial apparatus is widely utilized to investigate the influences of various loading histories on the re-liquefaction resistance of sands [5-9]. The development of column-like structure and connected voids in the strain hardening process could be responsible for the reduced reliquefaction resistance [8]. The induced anisotropic structure is extremely unstable and can be developed without much change in the relative density. Moreover, some undrained cyclic triaxial test results indicate that the development of anisotropy is continuous and orderly repeated during the whole liquefaction process [10]. The developed anisotropy is irreversible and remains in subsequent states. Compared with the triaxial device, the hollow cylinder torsional shear apparatus (HCTSA) can simulate more complicated stress paths and strain histories, in such a way that axial load, torque, internal and external pressures can be applied to a hollow cylindrical sample [11]. Recently, a set of torsional shear tests were conducted to investigate the effects of strain histories on re-liquefaction resistance of sands [12]. It was found that the intensity of residual shear strain significantly affects the reliquefaction resistance. For example, for dense samples with a relative density of 70%, the residual shear strain of 0.4% enhances the reliquefaction resistance, while the residual shear strain of 5.0% leads to a significant decrease in the reliquefaction resistance. Unfortunately, the sample is difficult to maintain geometry after experiencing large deformation in post-liquefaction by using flexible membranes in the tests. After two instances of liquefaction, the sample may collapse and the test cannot continue. To simulate multiple liquefaction events, researchers at the University of Tokyo developed a stacked-ring shear equipment [3]. The stacked rings can effectively restrain the lateral deformation of samples during each reconsolidation process. Hence, the soil sample can maintain its original geometry after multiple episodes of liquefaction and reconsolidation. However, the relatively large friction between the sample and stacked rings renders a nonuniform distribution of effective vertical stress in the soil, causing many uncertainty in the experimental analysis. In addition, only dry soil sample can be tested. The effect of undrained liquefaction is approximately by keep a constant volume of the sample.

In this study, a new stacked ring shear apparatus is developed by combining both advantages of an existing HCTSA and stacked rings. A pressure compensation technique is employed to reduce the friction between the membrane and stacked rings, with an aim to generate a uniform stress state to samples. A multiple liquefaction test was conducted to validate the pressure compensation technique and the capability of the new device to simulate multiple liquefaction events for saturated sands.

Although many of previous studies pointed out the important role of soil fabrics in multiple liquefaction process, they cannot be directly observed in laboratory tests. In recent years, Discrete element method (DEM) has become an efficient and direct way

to reveal the underlying micro-mechanism associated with the liquefaction responses [13][14][15]. A few studies were also devoted to study the multiple liquefaction process [16][17]. Yet, only simple spherical/circular particles were used in these studies. As one of the key challenges is to realistically simulate soil fabric during multiple liquefaction-consolidation process, in this study, we developed 3D clumped DEM to approximate the irregular shape of Toyoura sand particles, which is critical to realistically characterize fabric evolution and develop fundamental understanding and micromechanical insights into the multiple-liquefaction phenomenon.

2 The Staked Ring Torsional Apparatus

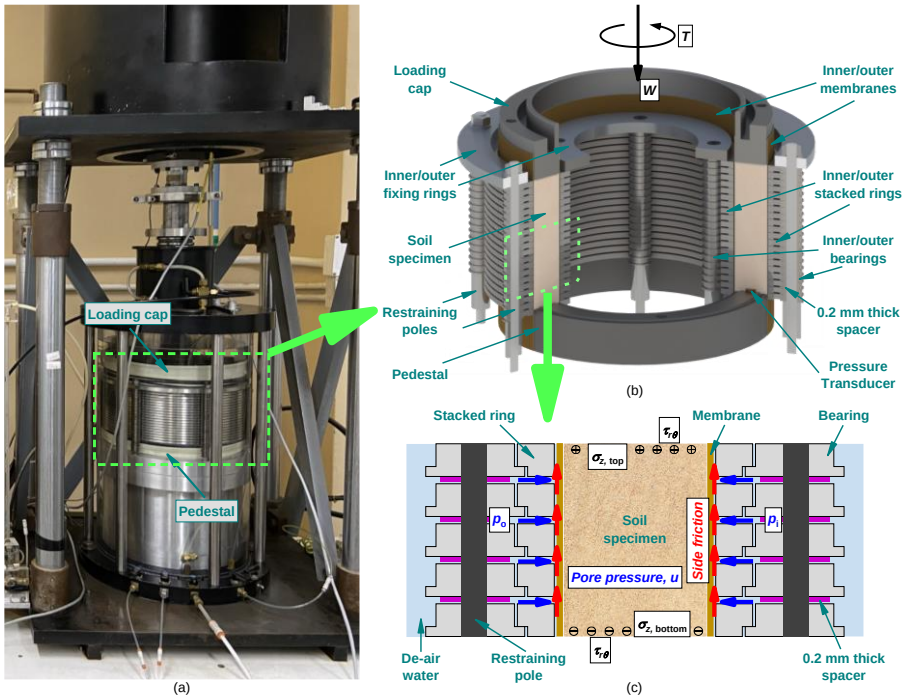

Fig. 1. (a) The loading system of hollow cylinder torsional shear apparatus at HKUST; (b) Schematic diagram of a new stacked-ring device, and (c) stress state of the sand sample placed in the new stacked-ring device.

The stacked ring torsional apparatus mainly includes two parts: an existing HCTSA and a new stacked-ring device. The loading cap and pedestal belong to the loading system of the existing HCTSA at the Hong Kong University of Science and Technology (HKUST), as shown in **Fig. 1(a)** [12,18, 19]. **Fig. 1(b)** illustrates the detailed structure of the new stacked-ring device. The new components including inner/outer stacked rings and restraining poles are newly designed according to the HCTSA dimension and

fabricated by the Design and Manufacturing Services Facility (DMSF) at HKUST. Each ring of inner/outer stacked rings is made of 5 mm thick stainless steel, and they are supported by specially designed bearings with a flange. Four inner and six outer poles are installed to restrain the bearings and guide the rings move only in the horizontal plane. These bearings only provide a very small friction against rotation of the rings. A stainless-steel spacer is placed between the bearings to keep stacked rings separated vertically by less than 0.2 mm from each other. The soil sample is sealed by inner/outer membranes, with an inner diameter, an outer diameter, and a height of 150, 200, and 100 mm, respectively. The vertical stress at the top $\sigma_{z,\,top}$ is calculated based on a load cell installed above the main load shaft, while the vertical stress at the bottom $\sigma_{z,\,bottom}$ is measured through a pressure sensor placed on the bottom platen of the devise.

Fig. 1(c) illustrates stresses on the sand specimen in the stacked-ring device. Different from the HCTSA, the side friction generated between the rings and membranes due to the normal contact force, as shown by the red arrows in **Fig. 1(c)**, will result in a large vertical stress reduction and non-uniform distribution within the sample. Similarly, friction in the circumferential direction has an influence on the shear stress distribution. However, the experimental results showed that the circumferential friction is neglectable owing to the bearing system [3]. Therefore, the critical issue is how to effectively reduce the side friction and minimize the reduction on $\sigma_{z,\,bottom}$. The pressure compensation technique proposed in this study utilizes the application of inner p_i and outer water pressures p_o on the membranes to reduce the direct contact force between the rings and membranes such that the difference between $\sigma_{z,\,top}$ and $\sigma_{z,\,bottom}$ shall be smaller and the vertical stress distribution shall be more uniform. Moreover, some lubricants commonly used in the lab, such as oils and greases, shall be applied on the surface of membranes to further eliminate the friction effect.

3 Multiple Liquefaction Tests

3.1 Testing Procedure

Toyoura sand used in all tests is a standard sand with angular to subangular particles. Its mean particle diameter D_{50}, specific gravity G_s, maximum void ratio e_{max}, and minimum void ratio e_{min} are 0.22 mm, 2.65, 0.988, and 0.640, respectively. Toyoura sand was dried at about 105℃ for 24 hours and then utilized to prepare the specimen adopting a dry deposition method. The specimen was divided into four layers with equal mass and poured layer by layer into the hollow space between inner and outer stacked rings using a funnel. A rubber hammer was utilized after preparing each layer to tap the inner/outer stacked rings for adjusting the relative density (D_r) to the expectant value. Carbon dioxide and de-air water were circulated through the specimen from the bottom toward the top for 2 hours and for 1 hour, respectively. A back pressure of 100 kPa was applied to the specimen to obtain full saturation and the B-value of greater than 0.97.

Fig. 2 shows the typical shear stress τ and strain γ behaviors of specimens at each stage of multiple-liquefaction tests. Firstly, specimens underwent the initial isotropical consolidation within the effective mean principal stress (EMPS) p' of 100 kPa (from

Point A to Point B in **Fig. 2(a)**). Then, the vertical movement of the load shaft was restricted for simulating simple shear conditions. Cyclic torsional shear tests were carried out at a constant shear strain rate of 0.8%/min under an *undrained* condition and always started in the clockwise (CW) direction. The single-amplitude (SA) shear stress (τ_{SA}) was 20 kPa, and the corresponding cyclic stress ratio (CSR) is 0.2. As shown in **Fig. 2(b)** and **(c)**, once the double-amplitude (DA) shear strain (γ_{DA}) reached 7.5% (Point C), sand specimens were considered liquefied. After that, the specimens stopped being sheared and started to be reconsolidated isotropically back to the original p' of 100 kPa under a *drained* condition (from Point C&C' to Point D in **Fig. 2(a)**), and residual shear stress inside the specimens was removed simultaneously (from Point C to Point C' in **Fig. 2(b)**). The strain between Point C and Point C' is negligible. The subsequent liquefaction stages (the second to sixth stages) were continued through the same procedure as described above.

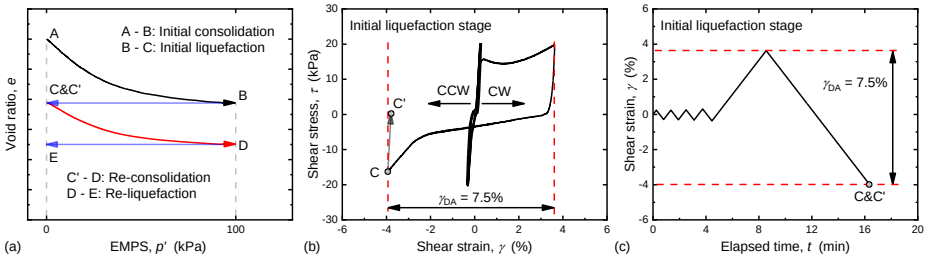

Fig. 2. Typical stage of multiple-liquefaction tests: (a) *e-p'* relation; (b) stress-strain relation; and (c) strain-time relation.

3.2 Testing Results

Fig. 3 presents the cyclic liquefaction behaviors at the first four stages of a multiple-liquefaction test with an initial D_r of 46.33%. In the first liquefaction stage, the specimen was in a virgin state, without any pre-shearing history. The sample experienced small-strain deformation until it suddenly reached a double-amplitude strain γ_{DA} of 7.5% due to flow liquefaction. The p' decreased gradually as the cycle number increases due to contractive tendency of the specimen. The relations between the excess pore-water pressure ratio (EPWPR) r_u, which is defined as the ratio of excess pore-water pressure (EPWP) Δu to the initial p', and γ in the different liquefaction stages are given in **Fig. 3(c)**. Before a Δu of 0.8, the γ increased slowly, and after which the γ accumulated progressively, known as cyclic mobility. After experiencing a flow state and partial hardening state, the first cyclic shearing was ended in the counter-clockwise (CCW) direction.

Due to the cumulative residual strain in previous liquefaction stages, an induced anisotropy inside the specimen affects its liquefaction behaviors in the subsequent liquefaction stages (which will be verified in the DEM study). As shown in **Fig. 3(a)**, in the second liquefaction stage, the specimen was liquefied in only half of the cycle. After the 2nd stage liquefaction, strong anisotropic fabric still remained in the sample, yet the

liquefaction resistance began to recover. The butterfly loops can be observed in the stress path of the third and fourth liquefaction stages given in **Fig. 3(b).** During the butterfly loop, shear strain continues to accumulate upon repeated cyclic stress, termed as "cyclic mobility" after initial liquefaction.

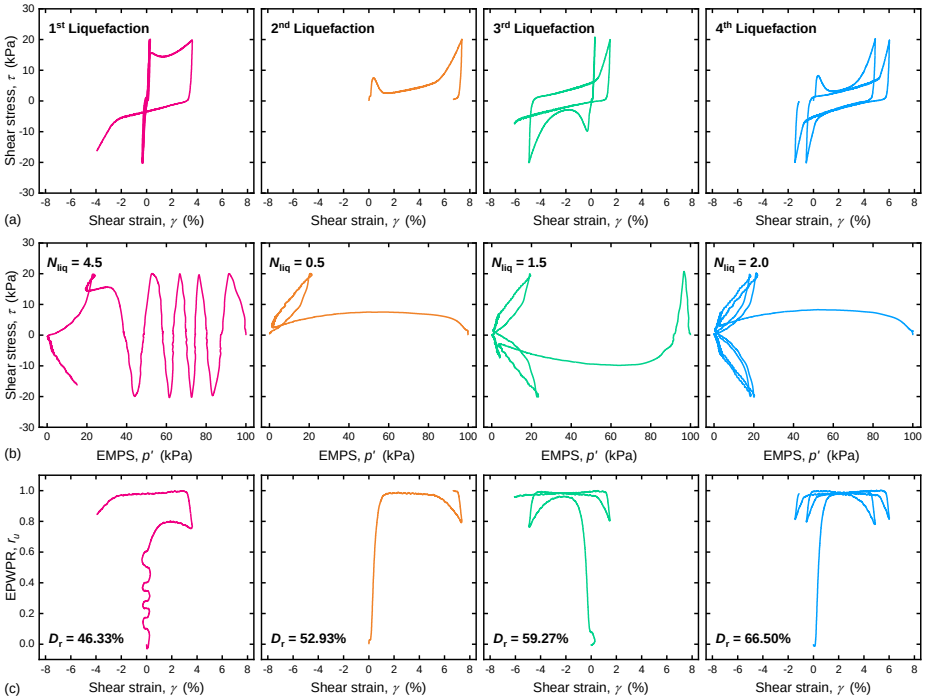

Fig. 3. Multiple-liquefaction behavior of Toyoura sand (the first to fourth liquefaction stages) (a) stress-strain relation; (b) stress path; and (c) EPWPR versus shear strain.

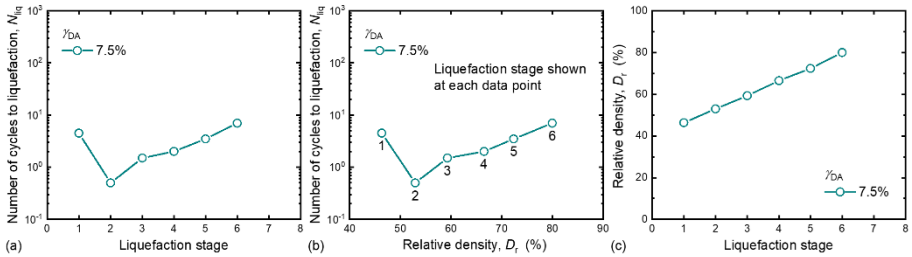

Fig. 4. Variations of (a) number of cycles to liquefaction with liquefaction stage; (b) number of cycles to liquefaction with relative density; and (c) relative density with liquefaction stage.

The number of cycles (N_{liq}) to γ_{DA} = 7.5% was used as an index to evaluate the liquefaction resistance of the specimen at each stage. The relation between the N_{liq} and

liquefaction stage was summarized in **Fig. 4(a)**. The liquefaction resistance is greatly reduced in the second liquefaction stage, but gradually increases as the liquefaction stage increases. The liquefaction resistance at the sixth stage is even slightly higher than the initial liquefaction resistance.

Fig. 4(b) and **(c)** show the relation between the N_{liq} and the relative density D_r, and the relation between the D_r and liquefaction stage, respectively. As the liquefaction stage progresses, the D_r continuously increases from 46.3% to around 80%. However, the liquefaction resistances at the 2nd to 5th liquefaction stages are smaller than the initial liquefaction resistance, even though their D_r values are significantly higher than the initial value. At the 6th liquefaction stage, D_r is almost twice of the initial D_r, yet, the liquefaction resistance is only slightly increased. Note that increase in N_{liq} is mainly due to increase in cyclic mobility. The resistance to initial liquefaction are very weak in all cases (see **Fig. 3**).

4 Discrete Element simulation

4.1 Clumped DEM packing

In this study, DEM simulations of multiple liquefaction stages are performed using an open-source code, Yade [20]. **Fig. 5(a)** shows a cubic DEM sample generated by 2940 clumped particles, and each clumped particle consists of 14 rigidly connected spheres. The density of each particle is 2650 kg/m^3, and Hertz-Mindlin contact model is used to describe the inter-particle contact relation, with Young's modulus of 70 GPa and Poisson's ratio of 0.15. **Fig. 5(b)** shows some selected examples of clumped particles, which could approximately represent the irregular shape of Toyoura sand. The equivalent diameter of each clumped particle, defined as the diameter of a sphere with the same volume as the corresponding clumped particle, ranges from 0.10 mm to 0.34 m, showing a good agreement with the experimental data [12], as shown in **Fig. 5(c)**.

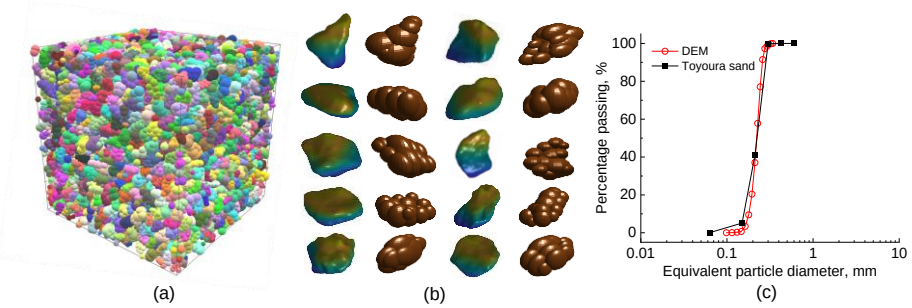

Fig. 5. (a) DEM clumped packing; (b) Examples of Toyoura sand particles models approximated by 14-sphere clumped particles; and (c) Particle size distribution of clumped particles and Toyoura sand particles [12].

4.2. Multiple liquefaction simulation

The clumped DEM can qualitatively to quantitatively reproduce the reliquefaction phenomenon. **Fig. 6** shows stress paths and stress-strain relations of sample with an initial relative density Dr =46.2% under cyclic stress ratio CSR=0.15 during the 1st, 2nd, 3rd, 6th and the 10th liquefaction stage. Note that a single-amplitude maximum strain of γ_{max} =5% was reached before each reconsolidation test. During each cyclic liquefaction test and reconsolidation test, the interparticle friction coefficient is chosen as 0.35.

In the 1st liquefaction stage, it's clear from **Fig. 6(a)** that the effective mean stress gradually decreases upon cyclic loading in the pre-liquefaction stage. After initial liquefaction, the soil sample is unable to sustain the cyclic loading, thus, large, rapid, and uncontrollable deformation develops, as shown in **Fig. 6(b)**. This phenomenon is referred to as flow liquefaction and often occurs in loose sands. At the 2nd liquefaction stage, although Dr increased to 51.6%, the effective mean stress decreased to zero almost in a half loading cycle (see **Fig. 6c)**, and flow liquefaction occurred after the initial liquefaction state was reached (see **Fig. 6d**). Thus, liquefaction resistance N_{liq} sigificantly decreased to 0.19. From the 3rd to 10th liquefaction stage, it's clear that initial liquefaction always happens in half a cycle of loading. The relative density increased significantly to 91.5% after nine reconsolidations, and the soil sample exhibits strong characteristics of cyclic mobility (see **Fig. 6h, 6j**), similar to the laboratory tests (**Fig. 3**)

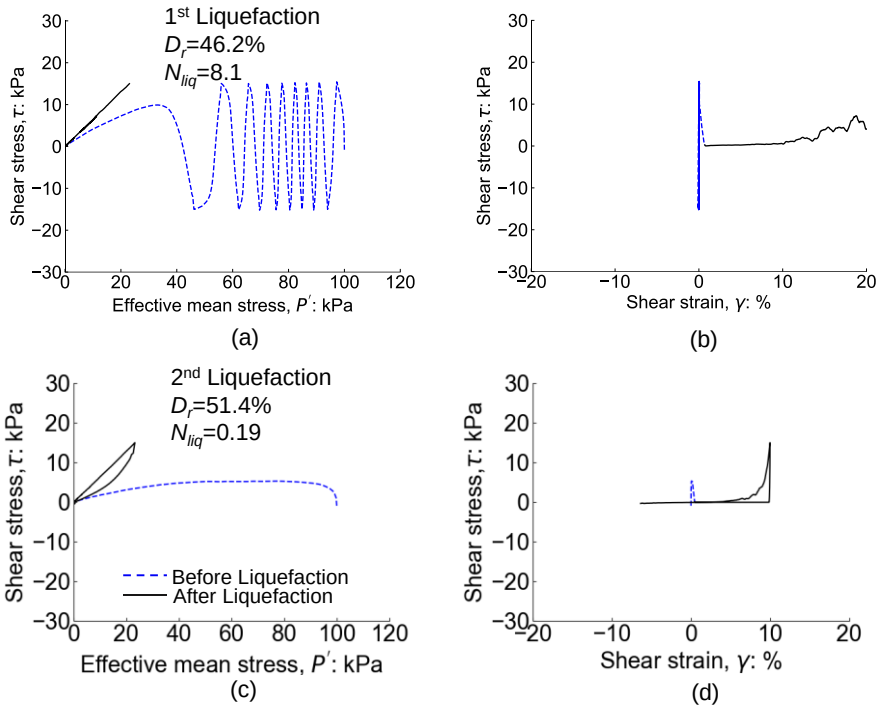

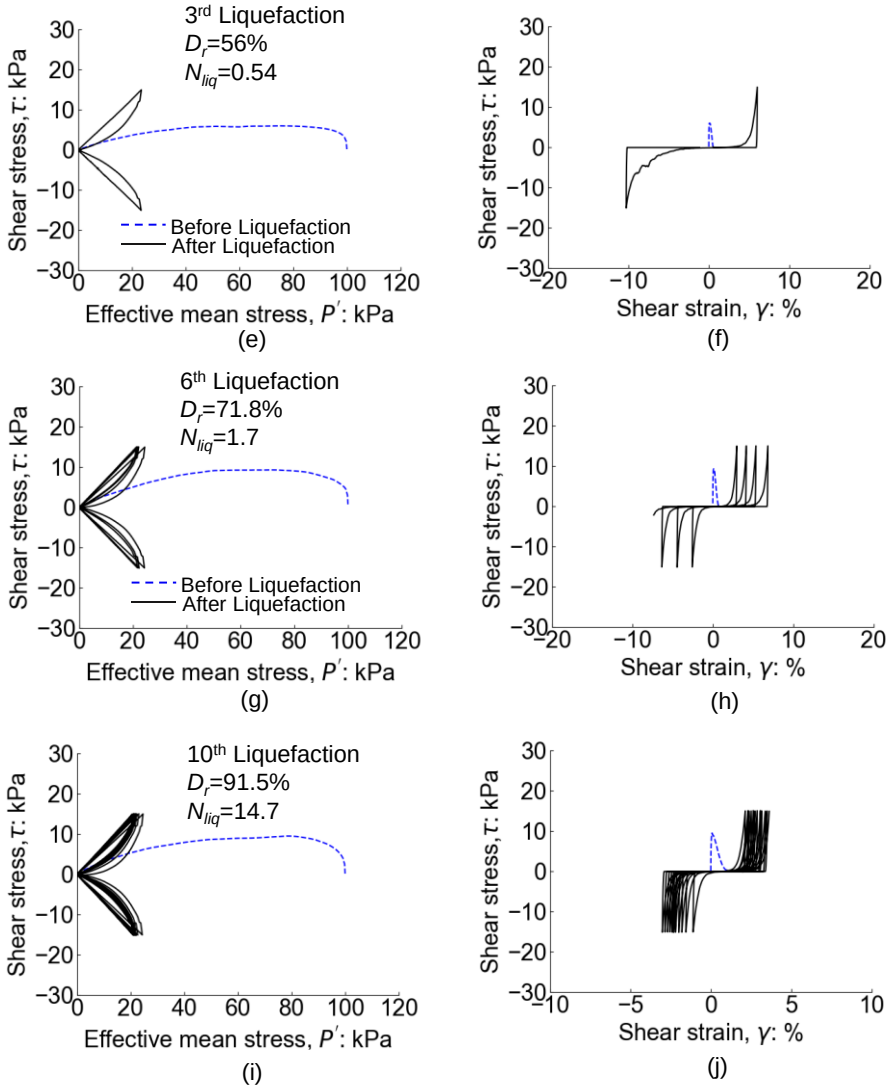

Fig. 6. DEM simulation of multiple-liquefaction response for the loose sand reconsolidated at γ_{max}=5% at a CSR= 0.15 during the 1st, 2nd, 3rd, 6th and 10th liquefaction stages: (a), (c), (e), (g) and (i): effective stress path; (b), (d), (f), (h) and (j): stress-strain curve.

Many DEM tests were conducted under different conditions, and the main results are summarized. **Fig. 7(a)** shows changes in the relative density D_r during each liquefaction stage (after the sample was reconsolidated under various γ_{max}). It is obvious that a larger maximum **shear** strain γ_{max} induces a higher rate of increase in D_r after each reconsolidation test. For example, D_r increased significantly from 46.2% to

91.5% after nine times of reconsolidation under γ_{max} =5%; whereas under a small strain level γ_{max} =0.3%, the relative density only slightly increases to 54.4%. The trend of volumetric compression is qualitatively comparable to experimental tests performed on Toyoura sand by Wahyudi et al. (2015), as shown in **Fig. 7(a)**. From this comparison, we concluded that using DEM-Clumps can correctly model the volumetric behavior during multiple liquefaction process, which is one of the key steps to obtain realistic fabrics through DEM simulation.

Fig. 7(b) shows the effects of γ_{max} on liquefaction resistance during multiple liquefaction stage. At a small strain level (γ_{max} =0.3%, 1%), the liquefaction resistance drastically increases at subsequent reliquefaction stages. However, when the soil sample experienced a large shear strain (e.g. γ_{max} =3%, 5%), the liquefaction resistance N_{liq} drops significantly to a very small value at the 2nd stage of liquefaction, and recovers afterwards together with densification of the soil sample in the 2nd to 10th stages of liquefaction/reconsolidation. Referring back to **Fig. 6**, under γ_{max} =5%, the initial liquefaction always happens in half a cycle of loading, even when Dr increased significantly to 91.5% after nine reconsolidations. The recovery of N_{liq} is mainly due to enhanced cyclic mobility (after initial liquefaction).

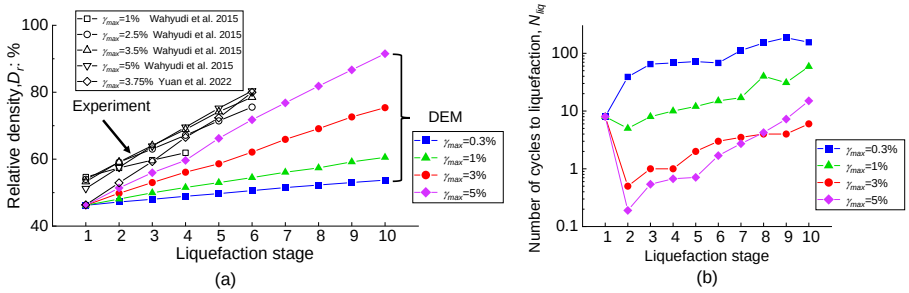

Fig. 7. (a) Relative density D_r ; and (b) Number of cycles to liquefaction N_{liq} in multiple liquefaction stage under various maximum shear strains γ_{max} at a CSR=0.15.

4.3. Evolution of soil fabrics and liquefaction resistance

Using DEM, the coordination number Z can be adopted to quantify the load-bearing structure of the clumped packing, where Z is defined as the averaged number of contacts per particle within the packing. In addition, a scalar quantity a_c can be defined to quantify the fabric anisotropy of the contact vector [13-15], whereas a larger a_c value represents a high anisotropy in load bearing structure. **Fig. 8** shows the effects of γ_{max} on soil fabrics (Z, a_c) after reconsolidation during multiple liquefaction stages. As shown in **Figs. 8(a) and (b)**, it is clear that when the soil sample experienced a small strain history (e.g. γ_{max} =0.3%), Z value gradually increases in subsequent liquefaction stages, while a_c value slightly reduced or remained largely unchanged. On the other

hand, for large maximum shear strains (e.g. γ_{max} =3% and 5%), *Z* decreases slightly and a_c increases markedly after the 1st reconsolidation, and then *Z* gradually increased while a_c was kept at a high value (e.g. when γ_{max} = and 5%, a_c value is always greater than 0.35). The above observation demonstrates that when soil sample experienced a small strain history (e.g. γ_{max} =0.3%), the contact number increased with a more isotropic load-bearing structure. However, under large γ_{max} , considerable anisotropic soil fabric was developed and remained in the subsequent liquefaction stage.

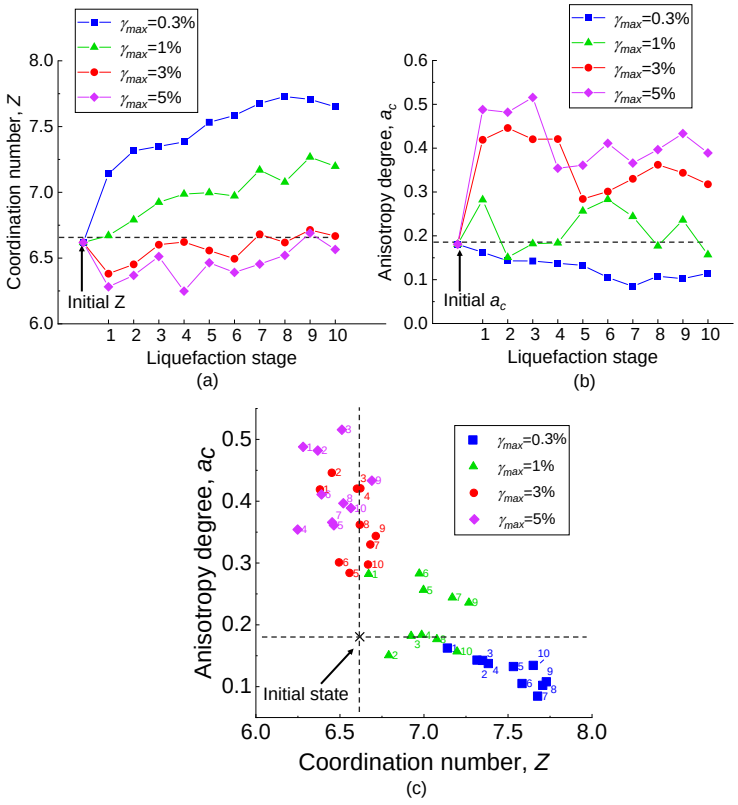

Fig. 8. (a): Coordination number *Z*; and (b): degree of anisotropy a_c after reconsolidation during multiple liquefaction stages; and (c): Relationship between a_c and Z under different maximum shear strain γ_{max} at a CSR=0.15.

Fig. 8(c) summarizes the correlation between coordination number Z and degree of anisotropy a_c of samples at the beginning of each liquefaction stages (right after reconsolidation from the previous liquefied state). Generally, Z and a_c show obvious negative correlation, i.e., an increase in a_c is associated with decrease in Z, and vice

versa. These two factors jointly affect the liquefaction resistance of the sample as shown in **Fig. 7.**

Figs. 9(a) and (b) summarize the relations between liquefaction resistance N_{liq} against Z, a_c under CSR=0.15 for samples with different γ_{max}. In general, N_{liq} exhibits a good correlation with Z and a_c after reconsolidation at various maximum shear strains. To be specific, when soil samples experienced a small strain γ_{max} = 0.30%, it can be observed from **Figs. 9(a) and (b)** that liquefaction resistance significantly increases during 2nd -10th liquefaction stage as compared with the 1st liquefaction resistance, which can be attributed higher Z values and lower a_c values as compared with those of the original packing (Z=6.62, a_c =0.18) after reconsolidation. On the other hand, when soil sample experienced a large maximum shear strains (e.g. γ_{max} = 3 and 5%), liquefaction resistance significantly reduces and this is due to substantial decrease in the number of inter-particles contacts (Z) and formation of a higher degree of fabric anisotropy after reconsolidation.

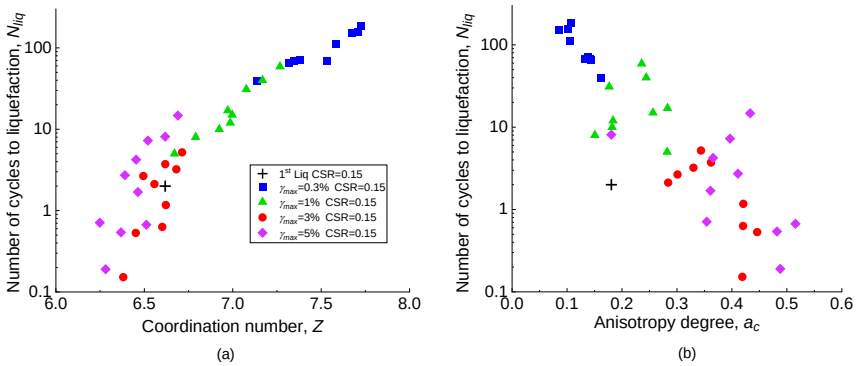

Fig. 9 Liquefaction resistance N_{liq} under CSR=0.15 versus (a): coordination number Z; and (b): degree of fabric anisotropy a_c.

5 Conclusions

In this study, a new stacked-ring torsional shear apparatus was developed to study the multiple liquefaction test of saturated Toyoura sand. 3D clumped DEM simulation were also performed to study the fabric evolution of the soil during the multiple liquefaction process. The main conclusions can be summarized as follows:

1. The developed stacked-ring torsional shear apparatus can be well utilized to study the multiple liquefaction behaviors of saturated sand. More tests need to be conducted to improve the uniform distribution of stress in the sample.
2. From the DEM study, it was observed that strain history due to prior liquefaction and reconsolidation can lead to significant change in soil fabrics, which have strong

correlation to the subsequent liquefaction resistance. Under large shear strains, the number of particle contact reduces, and a strongly anisotropic soil structure will be developed and retained in the subsequent liquefaction process, which dramatically reduces the liquefaction resistance. Increase in the relative density after reconsolidation can, to some extent, recover liquefaction resistance mainly through enhancing cyclic mobility in the post-liquefaction stage.

Acknowledgements

The study is supported by research grant No. 52179134 from National Natural Science Foundation of China, and grant No. 16214220 from Hong Kong Research Grants Council.

References

1. Kramer, S. L.: Geotechnical earthquake engineering. Pearson Education India (1996).
2. Yasuda, S., and Tohno, I.: Sites of reliquefaction caused by the 1983 Nihonkai-Chubu earthquake. Soils and Foundations 28(2), 61-72 (1988).
3. Wahyudi, S., Koseki, J., Sato, T., and Chiaro, G.: Multiple-liquefaction behavior of sand in cyclic simple stacked-ring shear tests. International Journal of Geomechanics 16(5), C4015001 (2016).
4. Cubrinovski, M., Henderson, D., and Bradley, B.: Liquefaction impacts in residential areas in the 2010-2011 Christchurch earthquakes. In: Proc., Int. Symp. on Engineering Lessons Learned from the 2011 Great East Japan Earthquake, pp. 811-824. Japan Association for Earthquake Engineering, Tokyo (2012).
5. Finn, W. D. L., Bransby, P. L., and Pickering, D. J.: Effect of strain history on liquefaction of sand. Journal of the Soil Mechanics and Foundations Division 96(6), 1917-1934 (1970).
6. Ishihara, K., and Okada, S.: Effects of stress history on cyclic behavior of sand. Soils and Foundations 18(4), 31-45 (1978).
7. Suzuki, T., and Toki, S.: Effects of preshearing on liquefaction characteristics of saturated sand subjected to cyclic loading. Soils and Foundations 24(2), 16-28 (1984).
8. Oda, M., Kawamoto, K., Suzuki, K., Fujimori, H., and Sato, M.: Microstructural interpretation on reliquefaction of saturated granular soils under cyclic loading. Journal of Geotechnical and Geoenvironmental Engineering 127(5), 416-423 (2001).
9. Sitharam, T. G., Vinod, J. S., and Ravishankar, B. V.: Post-liquefaction undrained monotonic behaviour of sands: experiments and DEM simulations. Géotechnique 59(9), 739-749 (2009).
10. Yamada, S., Takamori, T., and Sato, K.: Effects on reliquefaction resistance produced by changes in anisotropy during liquefaction. Soils and Foundations 50(1), 9-25 (2010).
11. Hight, D. W., Gens, A., and Symes, M. J.: The development of a new hollow cylinder apparatus for investigating the effects of principal stress rotation in soils. Géotechnique 33(4), 355-383 (1983).
12. Fardad Amini, P., Huang, D., Wang, G., and Jin, F.: Effects of strain history and induced anisotropy on reliquefaction resistance of toyoura sand. Journal of Geotechnical and Geoenvironmental Engineering 147(9), 04021094 (2021).

13. Wang, G., and Wei, J. T.: Microstructure evolution of granular soils in cyclic mobility and post-liquefaction process. Granular Matter 18(3), 51 (2016).
14. Wei, J. T., Huang, D. R., and Wang, G.: Microscale descriptors for particle-void distribution and jamming transition in pre- and post-liquefaction of granular soils. Journal of Engineering Mechanics 144(8), 04018067 (2018).
15. Wei, J. T., Huang, D. R., and Wang, G.: Fabric evolution of granular soils under multidirectional cyclic loading. Acta Geotechnica 15(9), 2529-2543 (2020).
16. Wang R, Fu P, Zhang, JM, Dafalias, YF: Fabric characteristics and processes influencing the liquefaction and re-liquefaction of sand. Soil Dyn Earthq Eng 125:105720 (2019)
17. Bokkisa, S., Wang, G., Huang, D., Jin, F.: Fabric evolution in post-liquefaction and re-liquefaction behavior of granular soils using 3D discrete element modeling. In Proc., 7th Int Conf., on Earthquake Geotechnical Engineering, 1461-1468. Rome, Italy (2019).
18. Yang, Z.: Investigation of fabric anisotropic effects on granular soil behavior. Doctoral dissertation, The Hong Kong University of Science and Technology, Hong Kong (2005).
19. Fardad Amini, P., Huang, D., and Wang, G.: Dynamic properties of Toyoura sand in reliquefaction tests. Géotechnique Letters 11(4), 1-8 (2021).
20. Šmilauer, V., Catalano, E., Chareyre, B., Dorofeenko, S., Duriez, J, Gladky, A., Kozicki, J., Modenese, C., Scholtès, L., Sibille, L., Stránský, J., Thoeni, K.: Yade documentation. In: Šmilauer V., (ed.) The Yade Project, 1st edn. http://yade-dem.org/doc/ (2010)